KDU Journal of Multidisciplinary Studies
(KJMS) Volume 6. Issue 2 Nov 2024
DOI: https://doi.org/10.4038/kjms.v6i2.126

KJMS 2024 VOL.6 (2): 30-41

GREEN SYNTHESIS OF MAGNETITE NANOPARTICLES USING *Syzygium aromaticum* FOR THE REMOVAL OF METHYLENE ORANGE

Gaminda K A P[1], Abeysinghe D T[1], Jayasinghe C D[2] and Senthilnithy R[1]

Department of Chemistry, The Open University of Sri Lanka, Nugegoda, Sri Lanka[1]
Department of Zoology, The Open University of Sri Lanka, Nugegoda, Sri Lanka[2]

ABSTRACT

Water contamination by textile dyes is a significant environmental issue, as these dyes are resistant to degradation and can have harmful ecological impacts. The present study focuses on using green synthesized magnetite nanoparticles using a sustainable method involving Syzygium aromaticum extract. These green-synthesized iron oxide nanoparticles (GMNPs) were tested for their ability to degrade methyl orange (MO) and compared to chemically synthesized zero-valent iron particles (CnZVIs). The study records that GMNPs were successfully synthesized, with particle sizes ranging from nano to micro scales. Within 20 minutes, 100 ppm of MO was reduced to 43 ppm and reached equilibrium at 120 minutes, with GMNPs removing up to 40 ppm of the dye. At equilibrium, approximately 59% of MO was removed using ~20 ± 1 mg of GMNPs, indicating they were more effective than CnZVIs. Kinetic studies indicated that the pseudo-second-order adsorption model (R^2 = 0.9993) was a better fit, while isotherm studies favored the Langmuir isotherm (R^2 = 0.9992) and Freundlich isotherm (R^2 = 0.9997). This suggests that the adsorption process was favorable for MO removal using GMNPs. Importantly, this research not only provides a promising solution to the problem of water contamination by textile dyes but also underscores the significant potential of GMNPs for environmental remediation, offering hope for a cleaner future.

KEYWORDS: *Green synthesis, Magnetite, S. aromaticum, Methyl orange, Cost-effective*

Corresponding Author: Abeysinghe D. T, Email: dtabe@ou.ac.lk

https://orcid.org/0000-0003-2454-5104.

1. INTRODUCTION

Azo dyes, widely used across several industries worldwide, cause significant environmental harm due to improper disposal. It has been found that approximately 20% of these dyes used in dyeing processes end up in wastewater, posing a grave threat to the environment (Basturk and Karatas, 2015). The azo bond, also known as N=N, is the chromophore responsible for the dazzling colors of these dyes (Phukan, 2015). Over the years, a plethora of azo dyes have been developed (Rahman, Abedin and Hossain, 2014) since Sir William Henry Perkin's (Perkin, 1856) discovery of the first synthetic dye in 1856 (Rahman, Abedin and Hossain, 2014). However, the rising demand for different dyes has significantly increased the percentage of azo dyes in wastewater. These harmful dyes are widely present in effluent sources such as textile, dyeing and printing, paper and ink manufacturing industries, and cosmetics. The release of azo dyes into the environment can cause severe damage to the ecosystem and living organisms.

Azo dyes are widely used in various industries, including cosmetics, textiles, and printing. However, they are known to be hazardous to human health and the environment. Azo dyes can cause skin cancers and other health problems, thus posing an occupational hazard for people working in dye-related industries. Therefore, researchers have developed effective methods for cleaning dye-contaminated wastewater for decades. Strategies such as ozonation, UV degradation, nanofiltration, membrane filtration, oxidation, adsorption, and electrocoagulation have been employed in the past (Dutta *et al.*, 2016). However, these methods have limitations in degrading azo dyes due to their resistivity. Biological treatment using microorganisms was also ineffective due to the low degradation activity. Therefore, researchers have turned to novel strategies to treat azo dye contaminations (Kobya *et al.*, 2014; Gao *et al.*, 2019). One promising method is the use of zero-valent iron nanoparticles (ZVINPs). ZVINPs have been recognized as a potential remediation to treat azo dye contamination (Iravani, 2011). Scientists discovered that zero-valent iron could reduce the azo bond (N=N) of the azo dye, causing discoloration (He *et al.*, 2012). Different strategies were developed to synthesize ZVINPs, including chemical and physical approaches. However, the utilization of these methods to synthesize ZVINPs is limited due to the cost and toxicity of the chemicals. Therefore, green synthesis emerged as an alternative approach to synthesizing ZVINPs due to its cost-effectiveness, eco-friendliness, non-toxicity, and utilization of bio-renewable natural sources (Huang *et al.*, 2014; Wang *et al.*, 2014; Abbasi Kajani and Bordbar, 2019; Gaminda *et al.*, 2023).

Recently, several research groups revealed the utilization of green synthesized nanomaterials to effectively remove azo dye (Beheshtkhoo *et al.*, 2018; Abbasi Kajani and Bordbar, 2019; Lohrasbi *et al.*, 2019; Khashij *et al.*, 2020; Yuan *et al.*, 2020; Khunjan and Kasikamphaiboon, 2021). Khunjan et al 2021 reported the synthesis of a novel Kaolin-supported nanoscale zero-valent iron (K-NZVI) using *Ruellia tuberosa* leaf extract to decolorize reactive black 5 (RB5) dye. The data showed that K-NZVI can decolorize the RB-5 with 92.1 – 99.8% efficiency. Bashir, et al. 2020 reported the development of iron nanoparticles using *Dimocarpus longan* extract to remove methyl orange (MO). The study revealed that green synthesized particles (DL-FeNPs) has achieved a 98.1% MO removal efficiency within 30 minutes. Beheshtkhoo group (Beheshtkhoo *et al.*, 2018) utilized the green synthesized iron oxide nanomaterials using leaf extract of *Daphne mezereum* to remove methyl orange. The decoloration efficiency was reported as 81.0% after 6 hours of incubation, the iron oxide nanoparticles with hydrogen peroxide (H_2O_2) treated MO. In green synthesis, various parts of the plant such as leaves, seeds, flowers, roots, etc., are used to prepare the green extract. The polyphenolic compounds in the green extract could act as a reducing agent to reduce metal ions and minimize the aggregation of the nanomaterials by acting as a capping/stabilizing agent. Various green extracts have been utilized to develop novel nanomaterials for multiple applications over time, and the functional properties of the green synthesized nanomaterials depend on the compounds available in the green extract. Furthermore, the size of the green

synthesized nanomaterials significantly depends on the capping/stabilizing agents in the green extract (Chen *et al.*, 2011). Over the years, different strategies have been developed to synthesize magnetite nanoparticles. However, to date, the synthesis of magnetite particles using a green approach, which indicates a comparison of chemical constituents, has not been reported.

Hence, our primary objectives are to synthesize novel iron oxide nanoparticles (GMNPs) using *Syzygium aromaticum* (clove) buds extract (water extract) and characterize the GMNPs using SEM, XRD, and FT-IR analysis. Lastly, we evaluated and compared the methyl orange degradation efficiency of GMNPs and chemically synthesized zero-valent iron particles (CnZVIs).

2. METHODOLOGY

A. Materials

Ferric chloride hexahydrate (with a purity of at least 99%, $FeCl_3 \cdot 6H_2O$), Sodium borohydride ($NaBH_4$), and Methyl orange (with an 85% purity, $C_{14}H_{14}N_3NaO_3S$) were acquired from Sigma Aldrich. Clove buds were sourced from local farms. All solvents essential for the experiments were prepared using distilled water.

B. Chemical synthesis of zero-valent iron particles and green synthesis of GMNPs

Zero-valent iron particles (CnZVIs) were chemically synthesized using a method reported by Rahman et al., 2014, using $FeCl_3.6H_2O$ and $NaBH_4$.

In this experiment, GMNPs were synthesized using the method reported by Gaminda et al 2024, using *Syzygium aromaticum* (clove) extract, $FeCl_3.6H_2O$, and NH_4OH. A precise amount of 1.0 grams of purified clove buds was carefully weighed and added to a flask containing 300.0 mL of distilled water. The mixture was heated to a temperature of 80°C and stirred continuously until the volume of the solution was reduced to 100.0 mL. The solution was then filtered using a gravity filtration process to remove any impurities and allowed to cool down to room temperature. Next, a 0.1 mol dm^{-3} $FeCl_3.6H_2O$ solution was prepared and mixed with the clove bud extract in a ratio of 1:2. The mixture was then stirred for 30 minutes at a controlled temperature of 60°C. During this process, the yellow color of the solution changed instantly to black, indicating the formation of iron oxide particles. In the next step, a 50 mL portion of 0.1 $moldm^{-3}$ $FeCl_3$ solution was mixed with 25.0 mL of the black color solution. The pH of the mixture was adjusted to 10 using NH_4OH, and the solution was continuously stirred for another 30 minutes at 60°C. This step facilitated the formation of iron oxide particles with improved purity and stability. Finally, the black color iron oxide particles were collected by gravity filtration and thoroughly washed with absolute ethanol and distilled water to remove any residual compounds of the extract. The particles were then dried using a vacuum oven for 12 hours at a temperature of 50°C.

C. Characterization

A range of characterization techniques were employed to analyze the properties of the synthesized nanomaterials, including a UV-visible spectrophotometer (UV-Vis), Fourier transform infrared spectroscopy (FT-IR), Scanning electron microscopy (SEM), and X-ray diffraction (XRD).

1. *UV-Vis spectroscopy*

The UV-visible spectrophotometer (ChromTech, CT-2600, Taiwan) was employed to analyze the absorption spectra of solutions treated with GMNPs and CnZVIs at 464 nm.

2. *Fourier transform infrared spectroscopy (FT-IR) analysis*

Fourier Transform Infrared Spectroscopy (FT-IR) was utilized to investigate the fabrication of GMNPs by the clove extract and CnZVIs, with measurements taken over the 4000 - 400 cm^{-1} range. The analysis was carried out using Bruker Vertex80 FT-IR spectrometer, Germany.

3. *Scanning electron microscopy (SEM) analysis*

The microstructure and size of the GMNPs were analyzed using scanning electron microscopy at different magnifications with an operating voltage of 20 kV (Carl Zeiss Evo 18 Research, Germany).

4. *X-ray diffraction (XRD) analysis*

X-ray diffraction (XRD) pattern was used to analyze the crystallinity state of GMNPs and CnZVIs with a Cu-K_β radiation source at room temperature, operating at 40Kv/30mA over a 2θ range of 5 to 80º, with a scanning speed maintained at 10 min^{-1}.

D. Batch experiment - Methyl orange (MO) degradation efficiency

A 100 parts per million (ppm) standard methyl orange (MO) solution was prepared by dissolving 25 mg MO in 250.0 mL of deionized water. A calibration plot was then developed using 5, 25, 50, 75, and 100 ppm concentrations. The unknown concentration was determined using the plot. According to the UV-Vis spectroscopy, the maximum wavelength (λ_{max}) for the MO was identified as 464 nm. Hence, the absorbance of the degraded MO solution was measured using a UV-spectrophotometer at 464 nm. The batch experiments were conducted using GMNPs and CnZVIs nanoparticles. A 25.0 mL of MO solution (100 ppm) was incubated with 20 ± 1 mg of GMNPs separately in 50 mL polypropylene plastic vials fitted with plastic caps. The solution was mixed using a thermo incubator at a speed of 150 rpm at a temperature of 25°C. One of the vials was withdrawn at a specific time interval (0, 20, 40, 60, 100, and 120 minutes), and the solution was filtered through Whatman filter papers (Grade 1) to remove the particles and measure the residual concentration of MO in the solution. The same procedure was followed using CnZVIs to evaluate the MO degradation efficiency.

The removal efficiency (η) and the amount of absorbed dye per unit mass of sorbent at a given time (q_t, mg/g) and equilibrium (q_e, mg/g) using GMNPs and CnZVIs were calculated by using the following equations (Wang and Li, 2013; Katata-Seru *et al.*, 2018; Gao *et al.*, 2019):

$$\eta = \frac{C_o - C_t}{C_o} \times 100\ \% \qquad (2)$$

$$q_t = (C_o - C_t)V/W \qquad (3)$$

$$q_e = (C_o - C_e)V/W \qquad (4)$$

Where η = the MO removal efficiency, C_o= the initial MO concentration in the solution (ppm), C_t = the MO concentration at a time (ppm), and C_e = the MO concentration at the equilibrium (ppm). All experiments were undertaken in triplicate, and the error values are less significant.

3. RESULTS AND DISCUSSION

A. UV-Vis spectroscopic analysis

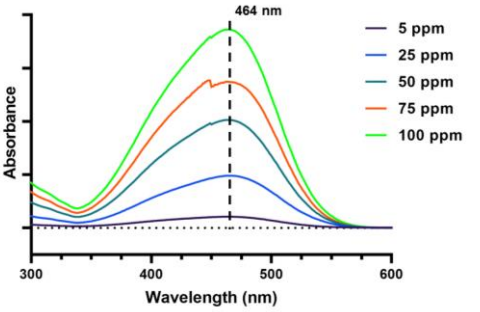

Figure 1. UV-Vis spectrum of the MO at different concentration

The UV-Visible spectroscopic analysis was performed to find the maximum wavelength (λ_{max}) of the MO solution. The UV-Vis spectrum indicated that 464 nm was the λ_{max} for the MO solution. The absorbance of the degraded MO solution in the presence of magnetite particles was then measured at a wavelength of 464 nm.

B. FT-IR analysis

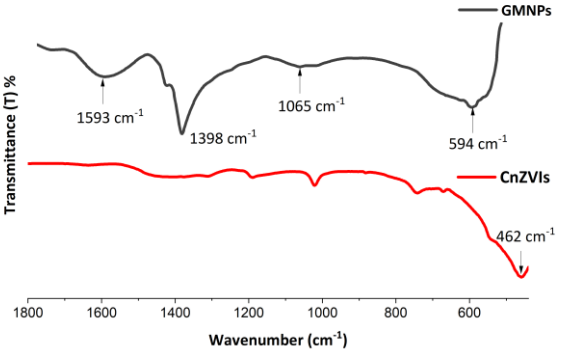

Figure 2. FT-IR spectrums of the GMNPs and CnZVIs

FT-IR analysis was conducted to assess the functional characteristics of iron nanoparticles. As illustrated in Figure 2, the peak observed at 594 cm^{-1} signifies the Fe-O stretching vibrations, affirming the GMNPs' formation through the constituents found in clove extract, supporting the idea that clove extract serves as both a reducing agent and a capping/stabilizing agent. The distinct peaks at 1065 cm^{-1} and another at 1593 cm^{-1} are associated with the C-N stretching vibrations of aliphatic amines and the C=C aromatic stretching vibration of GMNPs, respectively. The sharp peak at 1398 cm^{-1} corresponds to the -CH_2 groups (T. *et al.*, 2020; Parthipan *et al.*, 2021).

C. XRD analysis

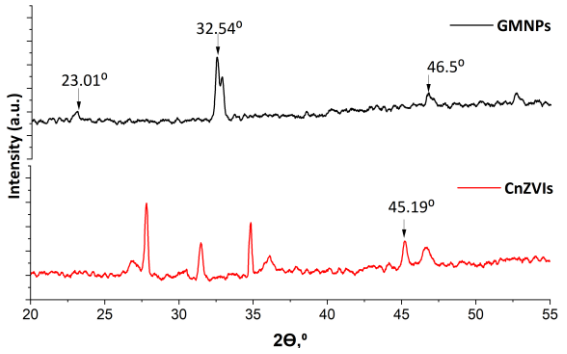

Figure 3. XRD pattern of the GMNPs and CnZVIs

These findings collectively validate the creation of GMNPs facilitated by the polyphenolic compounds in clove extract. Furthermore, in Figure 2, the peak at 462 cm^{-1} indicates the Fe-O stretching vibration of CnZVIs.

The X-ray diffraction (XRD) pattern, illustrated in Figure 3, of the green-synthesized iron nanoparticles (GMNPs) reveals a distinctive peak at 2Θ = 23.01º, corresponding to the characteristic absorption peak for polyphenols present in clove extract. This value aligns with previously reported data (Njagi *et al.*, 2011; Cao *et al.*, 2016). Additionally, the XRD pattern of the GMNPs displays a peak at 32.54º, corresponding to magnetite (Fe_3O_4). The peak at 32.54º corresponds to the Miller indices (hkl) values of 220, which denotes the crystalline phase of Fe_3O_4 (JCPDS/ICDD card No. 00-003-0862). The XRD pattern of the chemically synthesized iron nanoparticles (CnZVIs) exhibits a peak at 45.19º attributed to Fe^0 (Huang *et al.*, 2014). The peak at 45.19º corresponds to the hkl value of 110, which denotes the crystalline phase of Fe (JCPDS/ICDD card No. 00-001-1262). Consequently, both XRD and FT-IR data affirm the functionalization of GMNPs by the polyphenolic compounds in clove extract.

D. SEM analysis

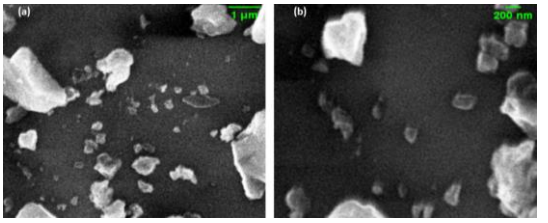

Figure 4. SEM images of GMNPs (a) 10 KX, and (b) 25 KX magnification

SEM images of GMNPs (Figure 4(a) and 4(b)) reveal irregularly shaped particles with a size distribution ranging from the nano to micro-scale, attributed to aggregation (Smuleac *et al.*, 2011). Furthermore, the broad size distribution of GMNPs from 70 nm to the micro-region may be attributed to the lower concentration of capping agents in the clove extract. The results confirm the successful synthesis of GMNPs utilizing clove extract, with SEM images supporting FT-IR analysis data.

E. Batch experiment - Methyl orange (MO) removal and kinetic studies

1. *Methyl orange (MO) removal*

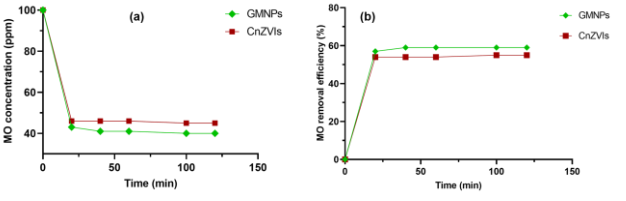

Figure 5. (a) MO concentration in the presence of GMNPs and CnZVIs with time and (b) MO removal efficiency of the GMNPs and CnZVIs

The removal of MO by GMNPs can be divided into two stages - an initial rapid removal stage followed

by a slower stage until the system reaches equilibrium over time. Figure 5(a) indicates that the concentration of MO declines with time and stabilizes at 120 minutes. After a 20-minute incubation period with GMNPs, the initial concentration of MO in solution was reduced to 43 ppm, ultimately reaching 40 ppm at equilibrium. Similarly, with CnZVIs, the initial concentration of MO in solution was 46 ppm, reaching 45 ppm at 120 minutes. In addition, as shown in Figure 5(b), MO removal efficiency by GMNPs and CnZVIs reached 57 % and 54 % at the 20-minute interval, respectively. At the equilibrium stage, MO removal efficiency reached 59 % and 55 %, respectively.

2. *Kinetic Studies*

The adsorption kinetics of MO onto the adsorbents (GMNPs and CnZVIs) were explored by applying pseudo-first-order and pseudo-second-order equations. These models rely heavily on the physical and chemical attributes of the adsorbent material. The pseudo-first-order model is particularly applicable at lower solution concentrations. The corresponding rate equation for the pseudo-first-order kinetics can be expressed as follows: (Wang *et al.*, 2014; Gao *et al.*, 2019):

$$\ln(q_e - q_t) = \ln q_e - k_1 t \qquad (5)$$

Where q_e and q_t (mg/g) are the amounts of MG molecules adsorbed on the GMNPs and CnZVIs at equilibrium and at different times t (min) and k_1 is the rate constant of the pseudo-first-order model for the adsorption process (min^{-1}). The linear plot of ln $(q_e - q_t)$ against time, as shown in Figure 6, was used to calculate the rate constant k_1. The slope of the linear plot gives the value for the k_1.

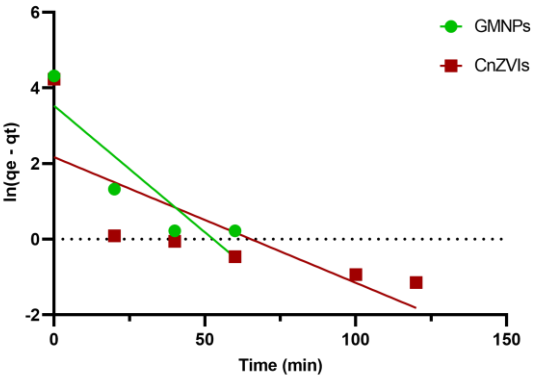

Figure 6. Pseudo-first order kinetics of the GMNPs and CnZVIs in the MO removal process

The pseudo-second-order kinetic model equation is expressed as follows (Bhattacharyya and Gupta, 2008; Gao *et al.*, 2019):

$$\frac{dq_t}{dt} = k_2 (q_e - q_t)^2 \qquad (6)$$

Integrating Eq. (6) by applying the boundary conditions t = 0 to t and q_t = 0 to t, gives:

$$\frac{1}{(q_e - q_t)} = \frac{1}{q_e} + kt \qquad (7)$$

When Eq. (7) linearized, it expressed as follows:

$$\frac{t}{q_t} = \frac{1}{k_2 q_e^2} + \left(\frac{1}{q_e}\right) t \qquad (8)$$

Where, q_e and q_t (mg/g) are the amounts of MG molecules adsorbed on the GMNPs and CnZVIs at equilibrium and at different times t (min) and k_2 (g $mg^{-1}min^{-1}$) is the rate constant of the pseudo-second-order model for the adsorption process. Values of the k_2 and q_e can be determined from the plot of t/qt against t, as shown in Figure 7.

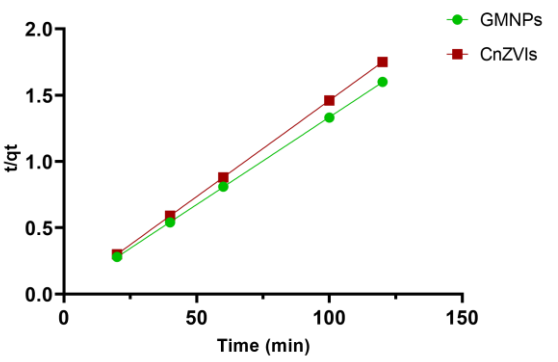

Figure 7. Pseudo-second-order kinetics of the GMNPs and CnZVIs in the MO removal process

Table1. The kinetic parameters of MO removal by GMNPs and CnZVIs

	Pseudo First Order		**Pseudo Second Order**	
	K_{obs} (min^{-1})	R_1^2	K_2 (g mg^1 min^{-1})	R_2^2
GMNPs	0.0276	0.5706	0.0188	0.9993
CnZVIs	0.0315	0.5979	0.0688	0.9999

The correlation coefficients (R^2) show that MO adsorption onto the GMNPs and CnZVIs was better fitted for the pseudo-second-order model (R^2 = 0.9993 and 0.9999, respectively) compared to the pseudo-first-order model, according to Table 1. Therefore, the adsorption of MO onto GMNPs did not follow the pseudo-first-order model but well-fitted the pseudo-second-order model.

3. *Adsorption model isotherms*

Adsorption isotherms are crucial for understanding the interaction between adsorbates and adsorbents, correlating parameters like adsorbate uptake (q_e) and equilibrium concentration (C_e), while keeping temperature and pH constant. They offer insights into adsorbent capacities, behaviors, and optimization of adsorption mechanisms. Various models, such as Langmuir and Freundlich, are commonly used in scientific literature to compare outcomes and understand sorption mechanisms due to their versatility. (Gao *et al.*, 2019; Sahoo and Prelot, 2020)

a) Langmuir model

The Langmuir model (Langmuir, 1916, 1917), initially designed for gas-to-solid adsorption, has been adapted for solid-liquid interfaces, especially for monolayer adsorption scenarios. This model quantifies the equilibrium between adsorbate and adsorbent by assessing surface coverage, dependent on adsorbate concentration. It assumes surface homogeneity, monolayer adsorption, and reversibility, neglecting lateral interactions among adsorbed molecules. Despite these simplifications, the Langmuir model is widely used and appreciated for effectively fitting various experimental datasets (Piccin, Dotto and Pinto, 2011; Gao *et al.*, 2019; Sahoo and Prelot, 2020). The following equation represents the expression for the Langmuir isotherm:

$$q_e = \frac{K_L Q_m C_e}{1 + K_L C_e}$$

where Q_m (mg/g or mol/g) and C_e (mol/L) are the maximum adsorption capacity and the concentration at equilibrium, respectively, and K_L is the Langmuir constant, which represents the energy of adsorption or the equilibrium constant of adsorbate-absorbent equilibrium (L/g or L/mol depending on the unit of Q_m and C_e).

This equation can be easily converted to linear forms:

$$\frac{1}{q_e} = \frac{1}{K_L Q_m C_e} + \frac{1}{Q_m}$$

The plot (Figure 8) of $1/q_e$ as a function of $1/C_e$ allows the determination of the Langmuir constants.

The adsorption characteristics of the Langmuir isotherm can be explained in terms of a dimensionless constant R_L. R_L or separation factor is defined as follows:

$$R_L = \frac{1}{1 + K_L C_e}$$

The R_L factor indicates if the adsorption process is favored or not. If $0 < R_L < 1$, adsorption is considered as favorable. It is irreversible for $R_L = 0$, unfavorable for $R_L > 1$, and linear adsorption when $R_L = 1$ (Piccin, Dotto and Pinto, 2011; Gao *et al.*, 2019; Sahoo and Prelot, 2020).

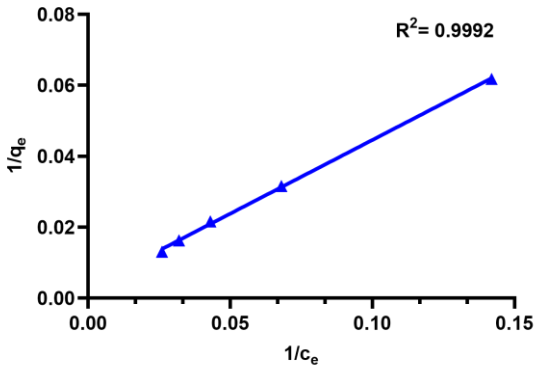

Figure 8. Langmuir isotherms for MO adsorption onto GMNPs, experimental conditions: T = 298 K, pH ~ 7.0

b) Freundlich model

The Freundlich isotherm elucidates reversible adsorption on surfaces with multiple layers under non-ideal conditions. It posits that each adsorption site exhibits a distinct binding energy, departing from a uniform distribution. This model reflects the heterogeneous nature of binding energies through an exponential function, mirroring real-world complexities (Piccin, Dotto and Pinto, 2011; Gao *et al.*, 2019; Sahoo and Prelot, 2020).

The following empirical equation represents the Freundlich isotherm:

$$q_e = K_F C_e^{-1/n}$$

where C_e is the equilibrium concentration of the adsorbate (mol/L). K_F and 1/n are the Freundlich constants representing the adsorption capacity and intensity, respectively.

The equation can be linearized by taking logarithms and is expressed as follows:

$$log(q_e) = logK_F + \left(\frac{1}{n}\right).logC_e$$

The representation of $\log(q_e)$ as a function of C_e (Figure 9) gives access to the K_F and n parameters. The value of 1/n gives characteristic information regarding the adsorption process. The 1/n value of less than 1 implies chemisorption or ordinary Langmuir isotherm, whereas 1/n above 1 indicates cooperative adsorption.

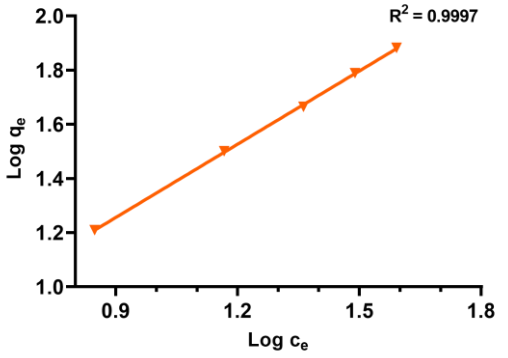

Figure 9. Freundlich isotherms for MO adsorption onto GMNPs, experimental conditions: T = 298 K, pH ~ 7.0

c) The Temkin isotherm model

The Temkin isotherm model suggests that the adsorption heat of all molecules decreases linearly as the adsorbent surface coverage increases. The model also assumes that the adsorption process is regulated by a uniform distribution of binding energies with a maximum binding energy (Piccin, Dotto and Pinto, 2011; Gao *et al.*, 2019; Sahoo and Prelot, 2020). The mathematical representation of the Temkin isotherm is shown in Figure 10:

$$q_e = \frac{RT}{b} lnK_T + \frac{RT}{b} lnC_e$$

where K_T is the equilibrium binding constant (L mol^{-1}) corresponding to the maximum binding energy, b is related to the adsorption heat, R is the universal gas constant (8.314 J K^{-1} mol^{-1}), and T is the temperature (K). Plotting q_e versus $\ln(C_e)$ results in a straight line of slope RT/b and intercept (RT ln KT)/b.

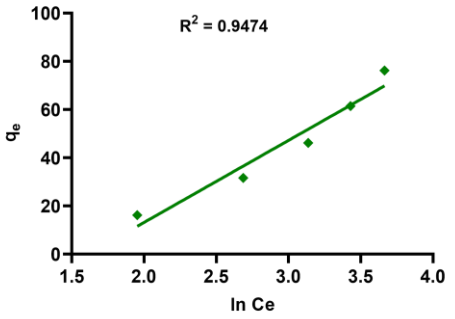

Figure 10. Temkin isotherms for MO adsorption onto GMNPs, experimental

Table 2. Langmuir, Freundlich, and Temkin parameters for the adsorption of MO by GMNPs

Isotherm model	Isotherm parameters	GMNPs
Langmuir	Q_m (mg/g)	327.33
	K_L (L/mg)	0.0074
	R_L	0.5761
	R^2	0.9992
Freundlich	K_F (mg/g)	2.7861
	n	1.1096
	R^2	0.9997
Temkin	K_T (L/mg)	5.0134
	b	35.03
	R^2	0.9474

Based on the isotherm data (Table 2), the Langmuir isotherm has a strong linear correlation for the adsorption of MO by GMNPs, with an R^2 value of 0.9992. The R_L value is approximately 0.57, which indicates that the adsorption process by the GMNPs is favorable. This observation suggests that the adsorption is homogeneous for MO in the solution. Furthermore, the 1/n values calculated from the Freundlich isotherm indicate that the removal of MO by the GMNPs follows the Langmuir isotherm/chemisorption, as the 1/n value is less than 1. Additionally, the heat sorption value 35.03 J/mol (0.0083 kcal/mol) calculated from the Temkin isotherm also suggests the physical adsorption of MO onto GMNPs. The positive value proposed by the heat sorption value of the Temkin isotherm suggests an exothermic process.

4. *Synthesis mechanism of GMNPs, and proposed adsorption mechanism for MO removal*

Based on the characterization data and the analysis data, a possible mechanism for the synthesis of GMNPs is proposed based on the published literature (Li, Elliott and Zhang, 2006; Wang *et al.*, 2014; Bashir, Ali and Farrukh, 2020; Gaminda *et al.*, 2024). Further, the kinetic data shows that the removal of MO follows the adsorption by the GMNPs and CnZVIs. Also, according to the reported studies, zero-valent iron particles can degrade the MO. The proposed mechanisms are described below, where the Ar stands for the phenyl group of the polyphenols.

Synthesis of GMNPs;

$$nFe^{3+} + Ar-(OH)_n \rightarrow nFe^{2+} + n(Ar=O) + nH^+$$

As previously mentioned, the synthesis of GMNPs is influenced by redox processes within the reaction, which hinge on the chemical species' standard reduction potentials (E^0). The standard reduction potential for Fe^{3+} is 0.77 V ($Fe^{3+} + e^- \rightarrow Fe^{2+}$). However, according to reported studies, the polyphenol-assisted reduction of Fe^{3+} to Fe^{2+} has been demonstrated (Eslami, Ebrahimzadeh and Biparva, 2018), and serves as evidence for the generation of Fe^{2+} through the reduction of Fe^{3+}, subsequently utilized as a precursor in the synthesis of magnetite via the co-precipitation method.

$$Fe^{2+} + 2Fe^{3+} + Ar-(OH)_n \rightarrow Fe_3O_4 - Ar = O (pH = 10)$$

(I) Adsorption of MO onto GMNPs,

$$Fe_3O_4 - Ar = O + MO \rightarrow Fe_3O_4 - Ar - O - MO$$

Recent studies (Li, Elliott and Zhang, 2006; Wang *et al.*, 2014; Bashir, Ali and Farrukh, 2020; Gaminda *et al.*, 2024) suggested that the zero-valent iron nanoparticles consist of the core-shell model. The core consists of zero-valent iron, and the shell is formed by the iron oxides/hydroxides formed due to the oxidation of the zero-valent iron.

In the first stage, Fe^{2+} is formed on the CnZVIs surface,

$$2Fe^0 + O_2 + 2H_2O \rightarrow 2Fe^{2+} + 4OH^-$$

$$Fe^0 + H_2O \rightarrow Fe^{2+} + H_2 + 2OH^-$$

In the second stage, Fe^{2+} oxidized to Fe^{3+},

$$4Fe^{2+} + 4H^+ + O_2 \rightarrow 4Fe^{3+} + H_2 + 2H_2O$$

In the third stage, Fe^{3+} reacts with OH^- and H_2O to form various hydroxides,

$$Fe^{3+} + 3OH^- \rightarrow Fe(OH)_3$$

$$Fe^{3+} + 2H_2O \rightarrow FeOOH + 3H^+$$

$$Fe(OH)_3 + 3H^+ \rightarrow FeOOH + H_2O$$

(II) Adsorption of MO onto CnZVIs particles,

$$Fe^0 - FeOOH + MO \rightarrow Fe^0 - FeOOH - MO$$

(III) Also, the partial reduction of the azo bond of the MO is possible due to the oxidation of the

CnZVIs (Beheshtkhoo *et al.*, 2018; Khashij *et al.*, 2020; Khunjan and Kasikamphaiboon, 2021),

$$Fe^0 \rightarrow Fe^{2+} + 2e$$

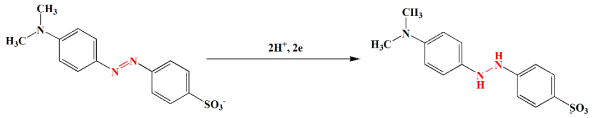

(IV) The degradation of the MO by the potent oxidant radicals is more likely as Fe^0 is a mild reductant, and iron corrosion promotes the generation of hydrogen peroxide in the presence of dissolved oxygen.

$$Fe^0 + O_2 + 2H^+ \rightarrow H_2O_2 + Fe^{2+}$$

$$2Fe^{2+} + O_2 + 2H^+ \rightarrow Fe^{3+} + H_2O_2$$

After, hydrogen peroxide and ferrous iron in the medium act as a Fenton catalyst system (Yuan *et al.*, 2020) and generate a strong oxidant of hydroxyl radical ($OH^{\cdot}$), which attacks the azo chromophore, causing decolorization.

$$Fe^{2+} + H_2O_2 \rightarrow Fe^{3+} + OH^{\cdot} + OH^-$$

$$MO + OH^{\cdot} \rightarrow OH^{\cdot} + CO_2 + H_2O + \text{mineralized products}$$

Further investigations are required to understand the mechanisms associated with the complete removal of the MO using green synthesized magnetite particles.

4. CONCLUSION

The current study demonstrates a successful method for synthesizing iron oxide nanoparticles (magnetite) utilizing *Syzygium aromaticum* extract. The clove extract's polyphenols significantly contributed to the reduction and capping of the nanoparticles during the synthesis process. FT-IR analysis confirmed the presence of various functional groups (polyphenols) from the clove extract on the nanoparticle surface. SEM images indicated that the nanoparticles exhibited irregular shapes and a range of sizes from approximately 70 nm to a micro-region, attributed to aggregation. XRD analysis further confirmed the identification of magnetite nanoparticles encapsulated by the polyphenols in the clove extract, as evidenced by the peak at 32.54º, characteristic of magnetite (Fe_3O_4).

Furthermore, batch experimental data revealed that the synthesized nanoparticles efficiently removed 100 ppm methyl orange (MO) from an aqueous solution using a 100 µL suspension (~20 ± 1 mg) of nanoparticles. This performance surpassed previously reported nanomaterials synthesized from other plant extracts. The MO removal efficiency by the nanoparticles reached 40 ppm (59% degradation efficiency), with an equilibrium time of approximately 120 minutes. Kinetic studies of the MO degradation indicated that the adsorption followed the pseudo-second-order model with an R^2 value of 0.9993. Isotherm studies revealed the superiority of the Langmuir isotherm in fitting the data (R^2= 0.9992) and the favorable R_L value (~0.57), along with the Freundlich isotherm with an R^2 value of 0.9997. These results signify the favorability of the adsorption process in MO removal using the synthesized iron oxide nanoparticles. The synthesized nanoparticles show great potential for removing methyl orange dye and improving water quality. Further research is required to optimize the reaction conditions and understand the nanoparticles' reactivity for removing various pollutants from wastewater.

5. ACKNOWLEDGMENT

Financial support for the research was provided by the Development-Oriented Research Grant 28 of The Open University of Sri Lanka, through the Accelerating Higher Education Expansion and Development (AHEAD) initiative in Sri Lanka.

6. REFERENCES

Abbasi Kajani, A. and Bordbar, A.K. (2019). 'Biogenic magnetite nanoparticles: A potent and environmentally benign agent for efficient removal of azo dyes and phenolic contaminants from water', *J. of Hazardous Materials*, 366, pp. 268–274.

Bashir, M., Ali, S. and Farrukh, M.A. (2020.) 'Green Synthesis of Fe_2O_3 Nanoparticles from Orange Peel Extract and a Study of Its Antibacterial Activity', *J.*

of the Korean Physical Society, 76(9), pp. 848–854.

Basturk, E. and Karatas, M. (2015). 'Decolorization of antraquinone dye Reactive Blue 181 solution by UV/H2O2 process', *J. of Photochemistry and Photobiology A: Chemistry*, 299, pp. 67–72.

Beheshtkhoo, N. *et al.* (2018). 'Green synthesis of iron oxide nanoparticles by aqueous leaf extract of Daphne mezereum as a novel dye removing material', *Applied Physics A: Materials Sc. and Processing*, 124(5), p. 0.

Bhattacharyya, K.G. and Gupta, S. Sen (2008). 'Adsorption of a few heavy metals on natural and modified kaolinite and montmorillonite: A review', *Advances in Colloid and Interface Science*, pp. 114–131.

Cao, D. *et al.* (2016). 'Removal of phosphate using iron oxide nanoparticles synthesized by eucalyptus leaf extract in the presence of CTAB surfactant', *Chemosphere*, 159, pp. 23–31.

Chen, Z.X. *et al.* (2011). 'Removal of methyl orange from aqueous solution using bentonite-supported nanoscale zero-valent iron', *J. of Colloid and Interface Science*, 363(2), pp. 601–607.

Dutta, S. *et al.* (2016) 'Rapid reductive degradation of azo and anthraquinone dyes by nanoscale zero-valent iron', *Environmental Technol. and Innovation*, 5, pp. 176–187.

Eslami, S., Ebrahimzadeh, M.A. and Biparva, P. (2018). 'Green synthesis of safe zero valent iron nanoparticles by: Myrtus communis leaf extract as an effective agent for reducing excessive iron in iron-overloaded mice, a thalassemia model', *RSC*.

Gaminda, K.A.P. *et al.* (2023). 'Degradation of Malachite Green using Green Synthesized Iron Nanoparticles by Coffea arabica Leaf Extracts and its Antibacterial Activity', *KDU J. of Multidisciplinary Studies*, 5(2), pp. 45–55.

Gaminda, K.A.P. *et al.* (2024). 'Green synthesis of iron nanoparticles using Syzygium aromaticum extracts and their applications: Nitrate removal, malachite green degradation and antibacterial activity', *Environmental Nanotechnol., Monitoring and Management*, 21, p. 100925.

Gao, S. *et al.* (2019). 'Adsorption of anionic dye onto magnetic Fe_3O_4/CeO_2 nanocomposite: Equilibrium, kinetics, and thermodynamics', *Adsorption Sc. and Technol.*, 37(3–4), pp. 185–204.

He, Y. *et al.* (2012). 'The comparative study on the rapid decolorization of azo, anthraquinone and triphenylmethane dyes by zero-valent iron', *Chemical Engineering J.*, 179, pp. 8–18.

Huang, L. *et al.* (2014). 'Green synthesis of iron nanoparticles by various tea extracts: Comparative study of the reactivity', *Spectrochimica Acta - Part A: Molecular and Biomolecular Spectroscopy*, 130, pp. 295–301.

Iravani, S. (2011). 'Green synthesis of metal nanoparticles using plants', *Green Chemistry*, 13(10), pp. 2638–2650.

Katata-Seru, L. *et al.* (2018). 'Green synthesis of iron nanoparticles using Moringa oleifera extracts and their applications: Removal of nitrate from water and antibacterial activity against Escherichia coli', *J. of Molecular Liquids*, 256, pp. 296–304.

Khashij, M. *et al.* (2020). 'Removal of reactive black 5 dye using zero valent iron nanoparticles produced by a novel green synthesis method', *Pigment and Resin Technol.*, 49(3), pp. 215–221.

Khunjan, U. and Kasikamphaiboon, P. (2021) 'Green Synthesis of Kaolin-Supported Nanoscale Zero-Valent Iron Using Ruellia tuberosa Leaf Extract for Effective Decolorization of Azo Dye Reactive Black 5', *Arabian J. for Science and Engineering*, 46(1), pp. 383–394.

Kobya, M. *et al.* (2014). 'Treatment of textile dyeing wastewater by electrocoagulation using Fe and Al electrodes: Optimisation of operating parameters using central composite design', *Coloration Technol.*, 130(3), pp. 226–235.

Langmuir, I. (1916). 'The constitution and fundamental properties of solids and liquids. Part I. Solids', *Journal of the American Chemical Society*, 38(11), pp. 2221–2295.

Langmuir, I. (1917). 'The constitution and fundamental properties of solids and liquids. II. Liquids', *Journal of the American Chemical Society*,

39(9), pp. 1848–1906.

Li, X.Q., Elliott, D.W. and Zhang, W.X. (2006) 'Zero-valent iron nanoparticles for abatement of environmental pollutants: Materials and engineering aspects', *Critical Reviews in Solid State and Materials Sciences*, 31(4), pp. 111–122.

Lohrasbi, S. *et al.* (2019). 'Green Synthesis of Iron Nanoparticles Using Plantago major Leaf Extract and Their Application as a Catalyst for the Decolorization of Azo Dye', *BioNanoScience*, 9(2), pp. 317–322.

Njagi, E.C. *et al.* (2011). 'Biosynthesis of iron and silver nanoparticles at room temperature using aqueous sorghum bran extracts', *Langmuir*, 27(1), pp. 264–271.

Parthipan, P. *et al.* (2021). 'Evaluation of Syzygium aromaticum aqueous extract as an eco-friendly inhibitor for microbiologically influenced corrosion of carbon steel in oil reservoir environment', *Bioprocess and Biosystems Engineering*, 44(7), pp. 1441–1452.

Perkin, W.H. (1856). 'Producing a new coloring matter for dyeing with a lilac or purple color stuffs of silk, cotton, wool, or other materials', *William Henry Perkin, United Kingdom, BP1984* [Preprint].

Phukan, M. (2015). 'Characterizing the ion-selective nature of Fe0-based systems using azo dyes: Batch and column experiments', *FOG - Freiberg Online Geosc.*, 42.

Piccin, J.S., Dotto, G.L. and Pinto, L.A.A. (2011). 'Adsorption isotherms and thermochemical data of FDandC RED N° 40 Binding by chitosan', *Brazilian J. of Chemical Eng.*, 28(2), pp. 295–304.

Rahman, N., Abedin, Z. and Hossain, M.A. (2014). 'Rapid degradation of azo dyes using nano-scale zero valent iron', *American J. of Environmental Sc.*, 10(2), pp. 157–163.

Sahoo, T.R. and Prelot, B. (2020). *Adsorption processes for the removal of contaminants from wastewater: The perspective role of nanomaterials and nanotechnology, Nanomaterials for the Detection and Removal of Wastewater Pollutants*. Elsevier Inc.

Smuleac, V. *et al.* (2011). 'Green synthesis of Fe and Fe/Pd bimetallic nanoparticles in membranes for reductive degradation of chlorinated organics', *Journal of Membrane Science*, 379(1–2), pp. 131–137.

T., S.J.K. *et al.* (2020). 'Biosynthesis of multiphase iron nanoparticles using Syzygium aromaticum and their magnetic properties', *Colloids and Surfaces A: Physicochemical and Eng. Aspects*, 603, p. 125241.

Wang, L. and Li, J. (2013). 'Removal of methylene blue from aqueous solution by adsorption onto crofton weed stalk', *BioResources*, 8(2), pp. 2521–2536.

Wang, T. *et al.* (2014). 'Green synthesized iron nanoparticles by green tea and eucalyptus leaves extracts used for removal of nitrate in aqueous solution', *Journal of Cleaner Production*, 83, pp. 413–419.

Yuan, M. *et al.* (2020). 'Green synthesized iron nanoparticles as highly efficient fenton-like catalyst for degradation of dyes', *Chemosphere*, 261, p. 127618.